Reaction of Hydroxyl Radical with Acetone. 1. Kinetics of the Reactions of OH, OD, and ^{18}OH with Acetone and Acetone-d_6

Tomasz Gierczak,[†] Mary K. Gilles,[‡] Stefan Bauerle, and A. R. Ravishankara*[,§]

Aeronomy Laboratory, National Oceanic and Atmospheric Administration, 325 Broadway, Boulder, Colorado 80305, and Cooperative Institute for Research in Environmental Sciences, University of Colorado, Boulder, Colorado 80309

Received: October 24, 2002; In Final Form: February 19, 2003

The rate coefficient for the reaction of OH with acetone, k_1, was measured by producing OH via pulsed laser photolysis and detecting it via laser-induced fluorescence to be $k_1(T) = 1.38 \times 10^{-13} + 3.86 \times 10^{-11} \exp(-1997/T)$ cm^3 molecule^{-1} s^{-1}. These results confirm the rate coefficient data of Wollenhaupt et al. (*J. Phys. Chem. A* **2000**, *104*, 2695). A value of k_1 suitable for atmospheric calculations is deduced from our data and that from previous work to be $k_1 = 1.39 \times 10^{-13} + 3.72 \times 10^{-11} \exp(-2044/T)$ cm^3 molecule^{-1} s^{-1}. The rate coefficients at 298 K for the reaction of OH with $CD_3C(O)CD_3$ (k_4), OD with $CH_3C(O)CH_3$ (k_2), and OD with $CD_3C(O)CD_3$ (k_5) were measured to be (in units of cm^3 molecule^{-1} s^{-1}) $(3.00 \pm 0.04) \times 10^{-14}$, $(2.07 \pm 0.14) \times 10^{-13}$, and $(3.26 \pm 0.16) \times 10^{-14}$, respectively; they were also measured at a few temperatures above and below 298 K. It was deduced that the reaction of ^{18}OH with acetone does not produce ^{16}OH. The large primary kinetic isotope effect (i.e., the large value of k_1/k_4 and k_2/k_5) at 298 K and its increase with decreasing temperature suggests that OH abstracts an H atom from acetone. k_1 was found to be independent of bath gas pressure between 1 and 490 Torr and independent of bath gas (He, N_2, or SF_6). The products and mechanism of the OH−acetone reaction is discussed in the companion paper.

1. Introduction

Acetone is one of the most important trace organic compounds in the free troposphere. Its average concentration of ∼0.5 ppbv makes it one of the most abundant organic compounds in clean air.[1−4] It is believed that acetone is a source of HO_x and its degradation products can help sequester NO_x in the upper troposphere.[5−7] Hence, the fate of acetone in the troposphere must be investigated. The two major pathways for atmospheric removal of acetone are photolysis and reaction with the hydroxyl radical, OH. The atmospheric photochemistry of acetone has been explored.[8−10] The rate coefficient, k_1, for reaction of OH with acetone

$$OH + CH_3C(O)CH_3 \rightarrow \text{products} \qquad (1)$$

has been the subject of previous investigations. We initiated the studies of the kinetics a few years back and reported our results on k_1 at an international gas kinetics symposium.[11]

In this paper we present results on the temperature dependence of the rate coefficient for reaction 1. We were particularly interested in the rate coefficient behavior at low temperatures, down to 200 K, relevant to atmospheric chemistry. Wollenhaupt et al.[12] recently found that the Arrhenius relationship for k_1 is markedly nonexponential and suggested that a combination of abstraction and complex formation in reaction 1 could be the cause of the curved Arrhenius plot. Simple H-atom abstraction with positive temperature dependence was suggested to be dominant at high temperatures, with OH−acetone complex formation leading to a different set of products contributing more to the reaction at lower temperatures. A suggested possible mechanism for complex formation is OH addition to the carbon in the carbonyl group, yielding an α-hydroxyisopropoxy radical, $(CH_3)_2C(OH)O^{\bullet}$. This complex could then decompose via carbon−carbon bond fission to form acetic acid and methyl radical:

$$OH + CH_3C(O)CH_3 \rightarrow [(CH_3)_2C(OH)O^{\bullet}] \rightarrow CH_3 + CH_3C(O)OH \qquad (1a)$$

This lower temperature process was suggested to be in competition with an H-atom abstraction, leading to water and acetonyl radical:

$$OH + CH_3C(O)CH_3 \rightarrow H_2O + CH_3C(O)CH_2 \qquad (1b)$$

Wollenhaupt et al.[12] inferred from their data that at 280 K both mechanisms contribute about equally, while at 210 K the association complex production channel dominates and at 400 K the H-atom abstraction dominates. There have been a few studies on the products of reaction 1, which are described in the part 2 of this study.[13]

Accurate values of k_1 under atmospheric conditions, $190 < T < 320$ K, are essential for determining the atmospheric lifetime of acetone and calculating the flux of acetone required to maintain the observed levels of acetone in the atmosphere. Such information is needed for calculating the contribution of acetone to the chemistry of the atmosphere in general and the upper troposphere in particular.

* Corresponding author. Address: NOAA/ERL, R/AL2, 325 Broadway, Boulder, CO 80305. E-mail: ravi@al.noaa.gov.

‡ Current address: Chemical Sciences Division, Lawrence Berkeley National Laboratory, MS 6R2100, 1 Cyclotron Road, Berkeley, CA 94720.

† Permanent address: Department of Chemistry, Warsaw University, ul. Zwirki i Wigury 101, 02−089 Warsaw, Poland.

§ Also associated with Department of Chemistry and Biochemistry, University of Colorado, Boulder, CO 80309.

10.1021/jp027301a CCC: $25.00
Published on Web 06/04/2003

We present the results of our study on the kinetics, products, and mechanism of reaction 1 in two parts. In part 1 we present our result on the kinetics of reaction 1 and the atmospheric implications of the measured rate coefficients. In part 2,[13] we will present our results on the products and the mechanism of reaction 1.

Specifically, we present here the rate coefficients for reaction 1 and the reactions of isotopically labeled hydroxyl radicals with $CH_3C(O)CH_3$ and $CD_3C(O)CD_3$:

$$OD + CH_3C(O)CH_3 \rightarrow \text{products} \quad (2)$$

$$^{18}OH + CH_3C(^{16}O)CH_3 \rightarrow \text{products} \quad (3)$$

$$OH + CD_3C(O)CD_3 \rightarrow \text{products} \quad (4)$$

$$OD + CD_3C(O)CD_3 \rightarrow \text{products} \quad (5)$$

The rate coefficients for reactions 2−5 allowed us to explore both the primary and secondary kinetic isotope effects as well as the exchange reactions that could indicate the structure of an association complex. Such data was helpful in deducing a mechanism for reaction 1, which is discussed in the companion paper.[13]

2. Experiments

The rate coefficients k_1-k_5 were measured by producing the hydroxyl radicals by pulsed laser photolysis and detecting them by pulsed laser-induced fluorescence. The apparatus used for such measurements has been described in detail previously[14] and only a brief summary will be given here. The Pyrex reactor (length ca. 20 cm; internal volume 150 cm^3) was maintained at a constant temperature (199−383 K) by circulating fluid from a thermostated bath through its jacket. The temperature of the gas in the reaction zone was measured by a retractable shielded thermocouple. The temperature is estimated to be accurate to ±1 K.

Photolysis of HONO or DONO at 351 nm (XeF excimer laser) produced OH or OD. HONO (DONO) was prepared in situ by dropwise addition of an aqueous (H_2O or D_2O) solution of 0.1 M $NaNO_2$ into 10−30% H_2SO_4 (D_2SO_4). A small flow of He (∼1 sccm) over the solution carried HONO (DONO) into the reactor. At low reaction temperatures (<240 K), the He/HONO flow was passed through a coldfinger immersed in a dry ice−ethanol bath to remove H_2O (D_2O), which could enhance condensation of acetone on the walls of the cold reactor. The use of a long photolysis wavelength (351 nm) prevented photolysis of acetone.

The photolysis beam (351 nm) and probe laser beam (∼281.9 nm) were copropagated through the reaction cell in a direction orthogonal to that of the gas flow. The OH (OD) fluorescence was detected by a photomultiplier tube (PMT) perpendicular to both the laser beams and gas flow. The output of the PMT was processed by a gated charge integrator and read by a personal computer. At a given acetone concentration, the delay time between the photolysis and probe lasers was varied to obtain an OH temporal profile.

All experiments were carried out under pseudo-first-order conditions in OH or OD, i.e., $[OH]_0$ ($[OD]_0$) ≪ $[CH_3C(O)CH_3]$ ($[CD_3C(O)CD_3]$). The pseudo-first-order decay of OH is described by the following expression:

$$\ln\frac{[OH]_t}{[OH]_0} = -(k_i[X] + k_d)t = -k_i't \quad (I)$$

where t is the time between photolysis and probe laser pulses (i.e., the reaction time), k_i is the second-order rate coefficient, [X] is the concentration of acetone (acetone-d_6), and k_d is the rate coefficient for OH loss in the absence of acetone. A similar expression is valid for OD and ^{18}OH temporal profiles. In reactions where OH or OD were monitored, k_d was measured separately in the absence of acetone at the same bath gas pressure and photolyte concentration and was found to be first order in [OH] or [OD]. This loss was attributed to the reactions of OH (OD) with HONO (DONO) and impurities, as well as diffusion out of the detection zone. A plot of k_i' vs $[CH_3C(O)CH_3]$ or $[CD_3C(O)CD_3]$ yielded k_i as the slope. Typical k_d values ranged from 80 to 150 s^{-1}. In the case of ^{18}OH, k_d was measured to be ∼50 s^{-1} and was attributed to its loss via reaction with impurities and diffusion out of the volume where it was monitored.

The detection limit for OH, defined as $S/N = 1$, where S is the signal and N is equal to twice the standard deviation of the mean of the background, was ca. 2×10^9 radical cm^{-3} in 100 Torr of N_2 upon integration of 100 laser shots. We had excellent S/N for kinetics measurements since $[OH]_0$ was ca. 10^{11} radicals cm^{-3}. The signal-to-noise ratio was much better when He was used as the bath gas. $[OH]_0$ ($[OD]_0$) was estimated using the calculated HONO (DONO) concentration, the literature value[15] for the photolysis cross section of HONO, and the measured laser fluence. The HONO (DONO) concentration was calculated by assuming that the background OH loss rate coefficient, k_d, was only due to the reaction of OH with HONO (OD with DONO) and using the literature value[15] of the rate coefficient for the reaction of OH with HONO. Hence, $[OH]_0$ ($[OD]_0$) quoted in the tables of results are upper limits.

Measurement of k_3. The reaction of $O(^1D)$, produced by 248 nm (KrF laser) photolysis of O_3, with $H_2{}^{18}O$ was a source of ^{18}OH to measure k_3.

$$O_3 + h\nu \rightarrow O(^1D) + O_2 \quad (6)$$

$$O(^1D) + H_2{}^{18}O \rightarrow {}^{18}OH + {}^{16}OH \quad (7)$$

Since the ozone used as the photolytic precursor of $O(^1D)$ was not enriched in ^{18}O, equal initial concentrations of ^{16}OH and ^{18}OH were produced. The absorption lines of ^{16}OH and ^{18}OH are adjacent to one another (∼0.08 nm apart). Therefore, we could easily tune off ^{16}OH and on to ^{18}OH or vice versa.[16] For each concentration of acetone, we measured the pseudo-first-order rate coefficient for ^{16}OH decay, then tuned the probe laser on to an ^{18}OH transition, and measured the pseudo-first-order rate coefficient for the loss of ^{18}OH. Thus, k_1 and k_3 were measured together and the ratio of k_3/k_1 is quite accurate.

Knowledge of the exact acetone (acetone-d_6) concentration in the reaction cell, particularly at low temperatures, is crucial for accurate determinations of k_1-k_5. In our experiments, concentrations of acetone and its deuterated analogue were measured in the reaction cell itself by monitoring absorption of 184.9-nm light from a Hg pen-ray lamp propagated along the direction of the gas flow, orthogonal to the direction of the laser beams (see Figure 1). In almost all experiments, the absorption path length was 11.6 cm. The entire optical path was at the temperature of the measurements, and the temperature gradient along the optical path was negligible. The Hg lamp was blocked to avoid possible acetone photolysis at 184.9 nm while the OH temporal profiles were measured.

All experiments were carried out under slow flow conditions (linear flow velocities ∼10 cm s^{-1}). In most experiments, UHP N_2 (>99.999%) or He (>99.999%) was the buffer gas. The total

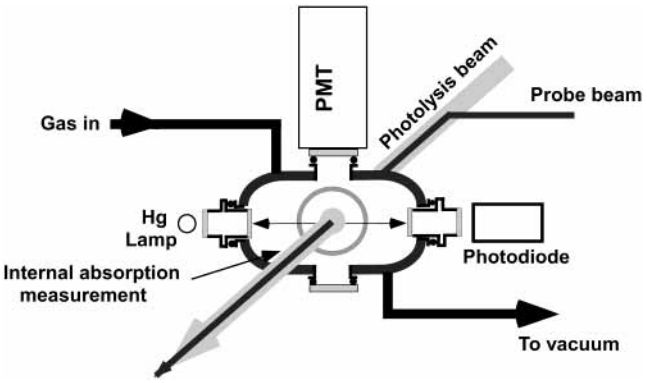

Figure 1. A schematic of the reactor used for measuring k_1-k_5 and the absorption cross sections of acetone and acetone-d_6.

TABLE 1: Absorption Cross Sections for Acetone and Acetone-d_6 at 184.9 nm as a Function of Temperature[a]

compd	T, K	$\sigma_{184.9nm} \pm 2\sigma$ (10^{-18} cm^2)	compd	T, K	$\sigma_{184.9nm} \pm 2\sigma$ (10^{-18} cm^2)
acetone	296	3.06 ± 0.03	acetone-d_6	295	4.01 ± 0.06
	296	3.01 ± 0.05		295	3.97 ± 0.10
	296	3.01 ± 0.02		295	3.77 ± 0.11
	296	2.95 ± 0.05		295	3.85 ± 0.12
	242	2.96 ± 0.03		295	3.88 ± 0.08
	231	2.98 ± 0.02		295	3.96 ± 0.08
	222	2.91 ± 0.07		273	4.08 ± 0.03
				253	4.31 ± 0.04
				242	4.41 ± 0.04
				232	4.61 ± 0.06

[a] The quoted errors are discussed in the text.

pressure was ~25, ~50, or ~100 Torr (measured with a calibrated capacitance manometer) with N_2 or He. A few experiments were carried out with SF_6 (>99.99%) as the buffer gas.

Measurement of the UV Absorption Cross Section of $CH_3C(O)CH_3$ and $CD_3C(O)CD_3$. The knowledge of the absorption cross sections of acetone and acetone-d_6 at 184.9 nm as a function of temperatures was essential for determining their concentration in the reactor. The cross sections were measured using a Hg pen-ray lamp, a photodiode, and the reactor (Figure 1) used for measuring k_1-k_5. First, the intensity of 184.9-nm radiation passing through the evacuated reactor, I_0, was measured. Then acetone (or acetone-d_6) vapor was flowed slowly through the reactor and the intensity, I, was monitored at several (up to 12) pressures. The pressure was measured by a calibrated 10 Torr capacitance manometer. The measured absorbance, $\ln(I_0/I)$, varied linearly with the pressure (concentration) of acetone (acetone-d_6) in the reactor. The absorption cross section was calculated from the slope of a plot of $\ln(I_0/I)$ vs [acetone] ([acetone-d_6]). Such measurements were carried out at various temperatures. The measured values are listed in Table 1 and are shown in Figure 2.

The absorption cross section of acetone at 184.9 nm decreased very slightly with decreasing temperature (Figure 2) and the average value was $(2.98 \pm 0.10) \times 10^{-18}$ cm^2. The quoted uncertainty is 2σ precision from the fit of $\ln(I_0/I)$ vs [acetone]. The decrease in the cross sections with temperature is smaller than the standard deviation of the mean quoted above. Therefore, we used this average value at all temperatures of the study. The average value is estimated to be uncertain by ~5%.

The 184.9-nm absorption cross section for acetone-d_6 noticeably increased with decreasing temperature (Figure 2). It was

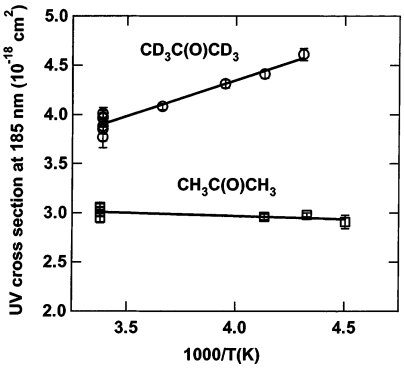

Figure 2. A plot of the measured UV absorption cross section of acetone and acetone-d_6 at 184.9 nm as a function of the reciprocal of temperature. The lines are fits of the measured cross sections to the expression $\sigma(T) = a + b \times (1000/T)$.

fitted to an equation of the form $\sigma(T) = a + b \times (1000/T)$ to yield

$$\sigma(T) = [(1.55 \pm 0.35) + (0.698 \pm 0.10) \times (1000/T)] \times 10^{-18}\ \text{cm}^2 \quad \text{(II)}$$

This equation was used for calculating $[CD_3C(O)CD_3]$ at various temperatures at which k_4 and k_5 were measured. The difference between the absorption cross sections of acetone and acetone-d_6 are not surprising, given that the cross sections of acetone are changing sharply around 184.9 nm while those of acetone-d_6 are not. Also, previous work at wavelengths close to 184.9 nm clearly show a shift in the spectra of acetone-d_6 relative to acetone.[17-19] Therefore, the small differences in the temperature dependence of the absorption cross sections of the two compounds are also not surprising.

Both acetone (spectroscopic grade, minimum purity 99.5%) and acetone-d_6 (99.9% isotopic purity, >99.5% chemical purity) were degassed by several freeze−pump−thaw cycles and were analyzed for impurities using gas chromatography−mass spectrometry (GC/MS). The list of compounds detected by this analysis, the upper limits for their concentrations, and their expected contribution to the measured values of k_1-k_5 are listed in Table 2.

3. Results and Discussion

The rate coefficients k_1-k_5 were measured in the pulsed photolysis system in 25, 50, or 100 Torr of N_2 and He; a few experiments were carried out in SF_6 also. Measurements of k_1 in ~1−3 Torr of He using discharge flow chemical ionization mass spectrometry (DF−CIMS) are described in part 2.[13] Typical OH temporal profiles from the photolysis system are displayed in Figure 3. The temporal profiles were exponential for at least a 2-decade decrease in OH concentration and were described by eq I. At a given temperature, each bimolecular rate coefficient was determined by measuring approximately seven pseudo-first-order rate coefficients spanning more than a factor of 10 in acetone (acetone-d_6) concentration. Figure 4 shows plots of measured k_i' vs [acetone] at 298 and 213 K. The values of k_1-k_5 were derived from linear weighted (according to the precision of the k_i' values) least-squares analysis of k_i' vs [acetone] or [acetone-d_6]. The measured values of k_1-k_5 are presented in Tables 3 and 4 and are also shown in Figure 5.

During this study we measured the rate coefficients for reactions of OH, OD, and ^{18}OH with acetone and of OH and OD with acetone-d_6. We will first describe our results on k_1

TABLE 2: Impurities Present in Acetone and Acetone-d_6 Used in This Study as Measured via GC/MS along with the Estimated Contributions of the Impurities to Measured k_1 and k_5[a,b]

impurity	concn,[c] ppmv	% contribution to the overall rate coeff at 220 K[d]
	Acetone	
acetaldehyde	9	<0.1
acetic acid methyl ester	3	<0.1
2-butanone	12	<0.1
methyl isopropyl ketone	1	<0.1
2,4-pentanedione	2	<0.1
4-hydroxy-4-methyl-2-pentanone	18	0.1[e]
2,5-hexanedione	10	<0.1
	Acetone-d_6	
2-butanone	18	<0.3
2-pentanone	3	<0.2
3-pentanone	1	<0.2
2-hexanone	4	<0.4
1,1,1,3,3,5,5,5-octadeutero-4-hydroxy-4-(trideuteriomethyl)-2-pentanone	9	<1.2[e]
dodecane	3	<0.6

[a] A 100 m nonpolar column (SPB-1, 0.32 mm, 1 μm film thickness) was used. First the column temperature was held at 40 °C for 8 min and then ramped up to 220 °C at a rate of 8 °C min^{-1}. The MS was operated in the scan mode (m/z = 40−250) with electron impact ionization (70 eV). [b] Besides those listed in this table, a few other compounds were also detected in trace quantities (<0.1 ppmv). [c] Concentrations of the impurities quoted in the table are approximate, because standards were not used for each of the detected impurities. The intensity of a GC/MS signal is a complicated function of several different physical parameters and it is difficult to calculate correction factors accurately. In general, the correction factors for calculating concentrations would be from 0.5 to 1, limiting the uncertainty in the concentrations to a factor of 2. For compounds heavier than the standards (acetone and methyl isobutyl ketone), the concentrations quoted are upper limits. [d] $k_{OH+acetone}(220\ K) = 1.4 \times 10^{-13}$ cm^3 molecule^{-1} s^{-1} and $k_{OH+acetone-d_6}(220\ K) = 1.6 \times 10^{-14}$ cm^3 molecule^{-1} s^{-1}. [e] $k_{OH+impurity}$ assumed to be $\sim 1 \times 10^{-11}$ cm^3 molecule^{-1} s^{-1}.

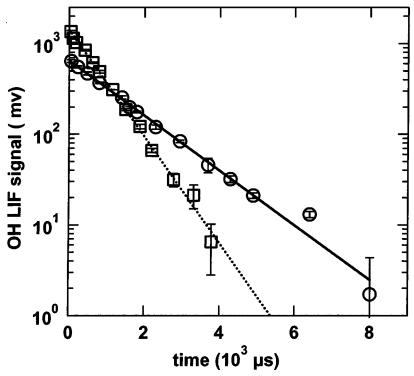

Figure 3. Temporal profiles of OH generated from the 351-nm photolysis of HONO at 296 K (squares: [acetone] = 6.6×10^{15} cm^{-3}) and 223 K (circles: [acetone] = 2.1×10^{15} cm^{-3}) in 100 Torr of N_2. The lines are weighted (according to S/N) linear least-squares fits to expression I.

and compare them with previous data. Then, we will describe our results on the reactions k_2-k_5. The possible mechanisms for this reaction are discussed in the companion paper.[13]

The rate coefficient for the reaction of OH with acetone, k_1, at 298 K is $(1.77 \pm 0.16) \times 10^{-13}$ cm^3 molecule^{-1} s^{-1}, as defined by eight separate measurements. The quoted uncertainty is 9% at the 95% confidence level and includes our estimated systematic errors. Figure 5 shows the temperature dependence of k_1 in an Arrhenius form. As can be seen from the figure, k_1

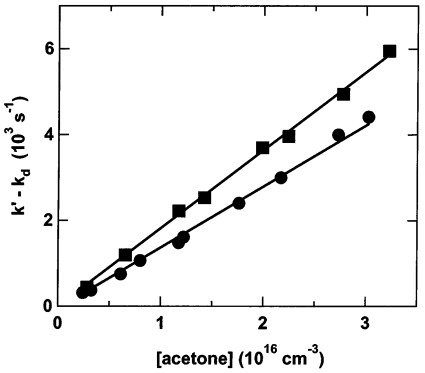

Figure 4. Plots of measured $k_i' - k_d$ vs [acetone] at 298 K (squares) and 213 K (circles). The lines are the linear least-squares fits to the expression: $k_i' - k_d = k_1$[acetone]. The slopes of the lines are values of k_1 at 298 and 213 K.

TABLE 3: Experimental Conditions and the Measured Value of k_1, k_2, and k_3 as a Function of Temperature[a]

T (K)	bath gas/ pressure (Torr)	[acetone] (10^{15} molecule cm^{-3})	$[OH]_0$ (10^{11} molecule cm^{-3})	k_1, k_2, or $k_3 \pm 2\sigma$ (10^{-13} cm^3 molecule^{-1} s^{-1})
		OH + Acetone (k_1)		
199	He/100	1.7−5.8	3.0	1.36 ± 0.10
208	He/100	2.0−12.3	2.8	1.46 ± 0.10
212	N_2/100	3.1−8.1	1.6	1.38 ± 0.07
213	N_2/100	3.9−5.9	2.8	1.51 ± 0.20[b]
223	N_2/100	3.1−26.2	1.8	1.41 ± 0.10
225	N_2/100	2.4−31.9	3.6	1.37 ± 0.08
232	N_2/100	4.3−46.2	2.2	1.37 ± 0.08[b]
238	He/1.1	0.02−0.33	2.0	1.49 ± 0.08[c]
244	N_2/100	3.5−43.4	1.7	1.44 ± 0.04
250	SF_6/490	4.6−29.1	5.0	1.48 ± 0.06
259	N_2/100	4.6−44.3	2.2	1.42 ± 0.02
271	N_2/100	4.0−42.8	1.8	1.55 ± 0.02
296	N_2/100	5.6−37.9	4.0	1.71 ± 0.03
296	N_2/100	2.8−32.2	1.0	1.79 ± 0.06
296	N_2/100	3.6−25.5	1.2	1.67 ± 0.06[b]
296	He/50	0.9−11.3	3.0	1.68 ± 0.12[d]
296	He/3	0.02−0.23	5.0	1.78 ± 0.10[c]
296	He/1.5	0.02−0.18	5.0	1.81 ± 0.18[c]
296	He/3	0.05−0.55	6.3	1.78 ± 0.10[c]
323	N_2/100	3.8−31.7	1.2	2.07 ± 0.05
333	He/3	0.04−0.25	1.7	2.46 ± 0.26[c]
353	He/1.5	0.02−0.14	4.0	2.74 ± 0.16[c]
356	N_2/100	3.0−32.1	1.0	2.80 ± 0.06
383	N_2/100	2.6−29.9	0.9	3.41 ± 0.14
		^{18}OH + Acetone (k_3)[d]		
240	He/50	1.4−11.2	1.3	1.43 ± 0.05
246	He/50	1.0−9.2	1.3	1.58 ± 0.06
252	He/50	1.2−10.3	1.7	1.50 ± 0.10
262	He/50	1.2−9.9	1.3	1.52 ± 0.05
296	He/50	0.8−11.3	3.0	1.85 ± 0.08
		OD + Acetone (k_2)		
223	He/50	2.0−22.3	2.5	1.78 ± 0.12
296	He/50	1.3−17.1	2.3	2.07 ± 0.14

[a] The quoted uncertainties are precisions of the slopes from the fits of k'_{1-3} vs [acetone] to a straight line. [b] Rate coefficients measured in the presence of 2×10^{17} cm^{-3} of O_2. [c] Discharge flow experiment (described in part 2).[13] [d] ^{16}OH and ^{18}OH were generated via 248-nm photolysis of a mixture of O_3, H_2O, or $H_2{}^{18}O$, and He.

obeys an Arrhenius relationship between 400 and 240 K. However, there is a marked deviation from the higher temperature Arrhenius behavior below 240 K, where k_1 reaches a near constant value of ca. 1.4×10^{-13} cm^3 molecule^{-1} s^{-1} down to 199 K.

In this study, we have measured k_1 using the pulsed photolysis LIF method and the DF−CIMS technique.[13] Both methods gave

TABLE 4: Experimental Conditions and the Measured Value of k_4 and k_5 as a Function of Temperature[a]

T (K)	bath gas/ pressure (Torr)	[acetone-d_6] (10^{15} molecule cm^{-3})	$[OH]_0$ (10^{11} molecule cm^{-3})	k_4 or $k_5 \pm 2\sigma$ (10^{-14} cm^3 molecule^{-1} s^{-1})
		OH + acetone-d_6 (k_4)		
211	He/50	3.2−19.6	4.0	1.60 ± 0.12
221	He/50	3.4−31.6	4.0	1.60 ± 0.12
233	He/50	1.9−30.8	3.0	1.39 ± 0.14
233	He/50	2.5−31.3	2.1	1.41 ± 0.18
244	He/50	2.3−29.2	1.9	1.72 ± 0.10
258	He/50	5.2−37.2	3.8	1.83 ± 0.18
295	N_2/100&25	4.4−32.0	1.8	3.00 ± 0.04
296	He/50	2.1−32.1	2.0	2.94 ± 0.42[b]
357	N_2/100	2.5−27.7	1.6	6.73 ± 0.26
383	N_2/100	3.9−25.3	1.7	9.57 ± 0.09
		OD + acetone-d_6 (k_5)		
213	He/50	2.1−22.5	2.9	2.23 ± 0.30
224	He/50	2.7−24.7	2.3	1.93 ± 0.12
233	He/50	2.6−31.2	2.3	2.04 ± 0.16
244	He/50	1.9−25.8	2.8	2.05 ± 0.16
266	He/50	2.1−32.6	1.6	2.19 ± 0.12
296	He/50	5.2−34.4	1.6	3.26 ± 0.16
324	He/50	1.3−14.7	1.5	5.04 ± 0.17

[a] The quoted uncertainties are precisions of the slopes of the fits of $k'_{4,5}$ vs [acetone-d_6] to a straight line. [b] OH was generated via 248 nm photolysis of a mixture of O_3, H_2O, and He.

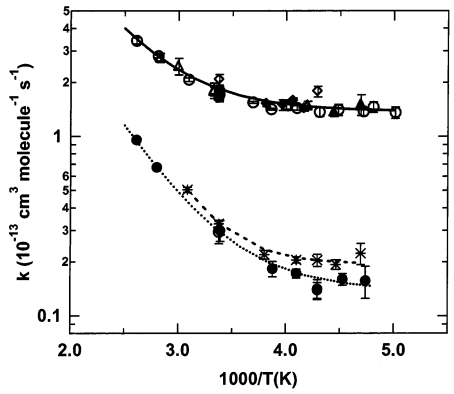

Figure 5. Plots of k_1 through k_5 (on a logarithmic scale) vs $1/T$. The lines are nonlinear least-squares fits of our data to eq III. The fit parameters for k_1 are shown in Table 5. The fitting procedure yielded the following expression for k_4 and k_5: $k_4(T) = 1.39 \times 10^{-14} + 2.05 \times 10^{-11}\exp(-2123/T)$ and $k_5(T) = 1.94 \times 10^{-14} + 1.99 \times 10^{-10}\exp(-2844/T)$ cm^3 molecule^{-1} s^{-1}. (k_1, open circles; k_1 in the presence of 2×10^{17} cm^{-3} of oxygen, filled triangles; k_1 (490 Torr of SF_6), open square; k_1 from DF−CIMS experiment, open triangles; k_2, open diamonds; k_3, hexagons; k_4, circle; k_5, stars).

the same values of k_1, indicating a lack of significant systematic errors. Furthermore, it is clear that k_1 is not dependent on pressure over the range from ∼1 to 490 Torr and it also does not depend on the nature of the bath gas (He, N_2, or SF_6).

Reaction 1 is relatively slow. Hence, impurities in the acetone sample may affect the measured value of k_1. If an impurity, present in sufficient concentration, reacts rapidly with OH, the measured value of k_1 could be erroneous; this could also lead to curvature in the Arrhenius plot. If the rate coefficient for the reaction of OH with the impurity had a negative activation energy, the curvature could be even more pronounced and could conceivably lead to the observed temperature independent values of k_1 at low temperatures (see Figures 5 and 6) even if the levels of impurities are low. Acetone and acetone-d_6 were analyzed for impurities using a GC/MS system. Table 2 lists the contribution of these impurities to the measured value of k_1 and

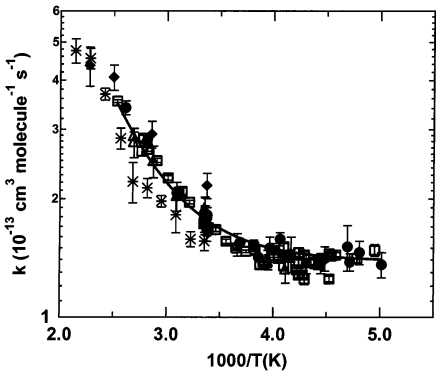

Figure 6. Plot of k_1 (logarithmic scale) vs $1/T$ from our studies and all other previous temperature dependence studies. (open squares, Wollenhaupt et al.;[12] open triangles, Le Calve et al.;[21] diamonds, Wallington et al.;[20] stars, Yamada et al.;[22] circles, this work; the solid line is the fit to the expression III). The most recent 298 K value of Vasvári et al. is also included as a square.

k_4. The net contribution is clearly less than 1% for k_1 and 3% for k_4, even at 220 K. Furthermore, if the impurities were the reason for the curvature, we would not get the large kinetic isotope effect, i.e., k_1/k_4, that we measured. On the basis of these arguments, we conclude that the observed curvature in the Arrhenius plot of k_1 is not due to reactive impurities.

First we compare our results with previous measurements. There are three previous measurements of k_1 as a function of temperature; their results are shown in Figure 6. Wallington and Kurylo[20] measured k_1 at five temperatures between 440 and 240 K. Their room-temperature value of k_1 is $(2.16 \pm 0.15) \times 10^{-13}$ cm^3 molecule^{-1} s^{-1}, which is ∼20% higher than ours. As seen in Figure 6, their measured values at other temperatures are close to those in the present study. They fit their measured values of k_1 at five temperatures to an Arrhenius relationship. More recently, La Calve et al.[21] reported k_1 between 372 and 243 K. Their room-temperature rate coefficient, $(1.84 \pm 0.25) \times 10^{-13}$ cm^3 molecule^{-1} s^{-1}, is only 7% larger than our value. They also fit their measured rate coefficients to an Arrhenius expression. Wollenhaupt et al.[12] carried out an extensive study of k_1 between 395 and 202 K and reported that the Arrhenius plot for k_1 is curved. Their room-temperature rate coefficient, $(1.73 \pm 0.09) \times 10^{-13}$ cm^3 molecule^{-1} s^{-1}, is in excellent agreement with the present determination. Indeed, our data agrees extremely well with their values over the entire temperature range of the two studies. Had Wallington and Kurylo[20]or Le Calve et al.[21] measured k_1 below 240 K, they also would have observed the curved Arrhenius plots. The results of Le Calve et al.[21] were sufficiently precise to show a slight curvature, but they chose to fit their data to an Arrhenius expression. Very recently, Yamada et al.,[22] using the PP−PLIF technique, measured the temperature dependence for reaction 1 between 298 and 952 K. Their measured rate coefficients for reaction 1 between 298 and 390 K are systematically about 12% lower than those measured by us, but still agree within the combined uncertainty. They also measured the temperature dependence for k_4 between 298 and 710 K. These rate coefficients are also systematically lower than those measured by us. At 298 K their rate coefficient is about 30% lower than ours. The difference between their value of k_4 and ours decreases with increasing temperature such that their value is ∼11% lower than ours at 380 K, the highest temperature of our study. We do not know the reason for this discrepancy.

There are many previous reports of k_1 measured only at one temperature around 298 K. These reported values, except the

TABLE 5: Comparison of the Temperature Dependence of k_1 from the Present Work with Those from the Literature

k_1(298 K) (10^{-13} cm^3 molecule^{-1} s^{-1})	A (10^{-12} cm^3 molecule^{-1} s^{-1})	E/R (K)	method[e]	ref
2.16 ± 0.16	1.7 ± 0.4	600 ± 75	FP-RF	20
1.84 ± 0.24	1.25 ± 0.22	561 ± 57	PP-PLIF	21
1.73 ± 0.09	a	a	PP-RF/PP-PLIF	12
1.73 ± 0.05			DF-RF/DF-LIF	23
1.56 ± 0.08	b	b	PP-PLIF	22
1.77 ± 0.18	c	c	PP-PLIF/DF-CIMS	this work
1.78 ± 0.18	d	d		15

[a] Experimental data was fit to a double exponential equation to get $k(T) = 8.8 \times 10^{-12}\exp(-1320/T) + 1.7 \times 10^{-14}\exp(423/T)$ cm^3 molecule^{-1} s^{-1}. [b] Fit to a modified Arrhenius expression to get $k(T) = (3.99 \times 10^{-24})T^{4.00}\exp(453/T)$ cm^3 molecule^{-1} s^{-1}. [c] Experimental data was fit to eq III to get $k(T) = 1.38 \times 10^{-13} + 3.86 \times 10^{-11}\exp(-1997/T)$ cm^3 molecule^{-1} s^{-1}. [d] Experimental data from above studies (except Yamada et al.[22]) were fit to eq III to obtain $k(T) = 1.33 \times 10^{-13} + 3.82 \times 10^{-11}\exp(-2000/T)$ cm^3 molecule^{-1} s^{-1}. [e] FP, flash photolysis; PP, pulsed photolysis; DF, discharge flow; RF, resonance fluorescence; PLIF, pulsed laser-induced fluorescence; LIF, laser-induced fluorescence; CIMS, chemical ionization mass spectrometry.

very recent report of Vasvári et al.,[23] have been evaluated in previous recommendations;[15] we will not compare them here with our measured values. Vasvári et al.[23] reported k_1 to be (1.73 ± 0.05) × 10^{-13} cm^3 molecule^{-1} s^{-1} at 298 K; their value is in excellent agreement with ours.

For use in atmospheric modeling, we have fit the data from this work and three previous studies[12,20,21] of the temperature dependence of k_1 to eq III

$$k(T) = A + B\exp(-C/T) \qquad \text{(III)}$$

using a nonlinear least-squares routine and obtained $k(T) = 1.39 \times 10^{-13} + 3.72 \times 10^{-11}\exp(-2044/T)$ cm^3 molecule^{-1} s^{-1}. We did not include k_1 measured by Yamada et al.[22] in this fit. They measured k_1 only above 298 K and their values may not be the most appropriate for atmospheric calculations (<320 K). The above value of k_1 is almost identical to the recommendation of NASA/JPL-2000,[24] which included our data in deriving the recommended value. This expression is not meant to represent a specific mechanism for reaction 1 but is merely a way to represent the measured values of k_1.

Kinetic Isotope Effects. Figure 5 shows the temperature dependence of k_4 and k_5; clearly, these reactions also show curved Arrhenius behavior and essentially mimic the temperature dependence of k_1. However, these rate coefficients are significantly smaller than k_1 and k_2. The large values of k_1/k_4 and the increase in k_1/k_4 with decreasing temperature suggest a primary kinetic isotope effect (KIE). For example, k_1/k_4 is 5.9 ± 0.9 at 298 K and 8.6 ± 0.8 at 212 K. Yamada et al.[22] reported k_1/k_4 to be 6.8 ± 1.0 at 298 K, slightly higher than our value. The large values of k_1/k_4 suggest that the breaking of a C−H bond in acetone is the primary pathway or at least the rate-limiting step in the reaction of OH with acetone. The rate coefficient k_5, for reaction 5, can have contributions from abstraction and, possibly, from exchange of hydroxyl radical. The temperature dependence of k_5 is essentially identical to that of k_4, but k_5 is consistently 10−20% larger than k_4, over the temperature range examined here. Also, k_2 is larger than k_1. Slightly larger values of k_5 over k_4 and k_2 over k_1 are consistent with a secondary kinetic isotope effect involving a C−H bond breakage.[25]

4. Atmospheric Implications

On the basis of the work of Wollenhaupt et al.[12] and the present study, it is clear that the Arrhenius plot for reaction 1 is curved. The recommended temperature dependence for reaction 1 derived from this work and those from previous studies, and shown in Table 5, can be used for atmospheric modeling. (We have shown in part 2[13] that the presence of oxygen in the atmosphere will not significantly affect the rate coefficient for the loss of acetone via its reaction with OH.)

The two major processes for the removal of acetone from the troposphere are photolysis and reaction with hydroxyl radicals. The reaction with OH is more important lower in the troposphere. Use of the value of k_1 recommended here will slightly increase the acetone loss rate due to reaction with OH and elevate the altitude at which the rates of OH reaction and photolysis contribute equally toward removal of acetone from the troposphere. The large values of k_1 at lower temperatures will lead to larger loss rates of acetone from the atmosphere. Hence, to account for the observed acetone concentrations in the atmosphere, the source strengths will have to be slightly larger than what was previously estimated on the basis of the assumption of a linear Arrhenius plot; such a reassessment has been reported by Jacob et al.[26] using the data of Wollenhaupt et al.[12] In the upper troposphere, acetone photolysis is a significant source of OH. The increased values of the rate coefficient will not affect the calculated HO_x production rate because the reaction with OH is not a major loss process for acetone in this region and the calculations of OH production from acetone use the observed abundance of acetone.

As noted in Table 3, the value of k_1 does not depend on pressure, at least over the range encountered in the troposphere. Therefore, the value of k_1 obtained from expression III is applicable for the entire troposphere.

Acknowledgment. This work was funded in part by NOAA's Climate and Global Change program and in part by Health of the Atmosphere program. We thank Ranajit K. Talukdar for assistance with some of the experiments presented here. We also thank David C. McCabe for critical reading of the manuscript and for many valuable comments.

References and Notes

(1) Arnold, F.; Schneider, J.; Gollinger, K.; Schlager, H.; Schulte, P.; Hage, D. E.; Whitefield, P. D.; van Velthoven, P. *Geophys. Res. Lett.* **1997**, *24*, 57.

(2) Knop, G.; Arnold, F. *Geophys. Res. Lett.* **1987**, *14*, 1262.

(3) Singh, H. B.; O'Hara, D.; Herlth, D.; Sachse, W.; Blake, D. R.; Bradshaw, J. D.; Kanakidou, M.; Crutzen, P. J. *J. Geophys. Res.* **1994**, *99*, 1805.

(4) Singh, H. B.; Chen, Y.; Gregory, G. L.; Sachse, G. W.; Talbot, R.; Blake, D. R.; Kondo, Y.; Bradshaw, J. D.; Heikes, B.; Thornton, D. *Geophys. Res. Lett.* **1997**, *24*, 127.

(5) McKeen, S. A.; Gierczak, T.; Burkholder, J. B.; Wennberg, P. O.; Hanisco, T. F.; Keim, E. R.; Gao, R.-S.; Liu, S. C.; Ravishankara, A. R.; Fahey, D. W. *Goephys. Res. Lett.* **1997**, *24*, 3177.

(6) Singh, H. B.; Kanakidou, M.; Crutzen, P. J.; Jacob, D. J. *Nature* **1995**, *378*, 50.

(7) Wennberg, P. O.; Hanisco, T. F.; Jaegle, L.; Jacob, D. J.; Hintsa, E. J.; Lanzendorf, E. J.; Anderson, J. G.; Gao, R.-S.; Keim, E. R.; Donnelly,

S. G.; Negro, L. A. D.; Fahey, D. W.; McKeen, S. A.; Salawitch, R. J.; Webster, C. R.; May, R. D.; Herman, R. L.; Proffitt, M. H.; Margitan, J. J.; Atlas, E. L.; Schauffler, S. M.; Flocke, F.; McElroy, C. T.; Bui, T. B. *Science* **1998**, *279*, 49.

(8) Emrich, M.; Warneck, P. *J. Phys. Chem. A* **2000**, *104*, 9436.

(9) Gierczak, T.; Burkholder, J. B.; Bauerle, S.; Ravishankara, A. R. *Chem. Phys.* **1998**, *231*, 229.

(10) Warneck, P. *Atmos. Environ.* **2001**, *35*, 5773.

(11) Gierczak, T.; Ravishankara, A. R. Kinetics of the reaction of hydroxyl radicals with acetone. 16th International Symposium on Gas Kinetics, 2000, University of Cambridge, Cambridge, UK.

(12) Wollenhaupt, M.; Carl, S. A.; Horowitz, A.; Crowley, J. N. *J. Phys. Chem. A* **2000**, *104*, 2695.

(13) Talukdar, R. K.; Gierczak, T.; McCabe, D. C.; Ravishankara, A. R. *J. Phys. Chem. A* **2003**, *107*, 5021.

(14) Vaghjiani, G. L.; Ravishankara, A. R. *J. Chem. Phys.* **1989**, *93*, 1948.

(15) DeMore, W. B.; Sander, S. P.; Golden, D. M.; Hampson, R. F.; Kurylo, M. J.; Howard, C. J.; Ravishankara, A. R.; Kolb, C. E.; Molina, M. J. *Chemical Kinetics and Photochemical Data for use in Stratospheric Modeling*; Jet Propulsion Laboratory, 1997, JPL Publication 97-4.

(16) Vaghjiani, G. L.; Ravishankara, A. R.; Cohen, N. *J. Phys. Chem.* **1989**, *93*, 7833.

(17) Lawson, M.; Duncan, A. B. F. *J. Chem. Phys.* **1944**, *12*, 329.

(18) Robin, M. B.; Kuebler, N. A. *J. Mol. Spectrosc.* **1970**, *33*, 274.

(19) Ito, H.; Nogata, Y.; Matsuzaki, S.; Kuboyama, A. *Bull. Chem. Soc. Jpn.* **1969**, *42*, 2453.

(20) Wallington, T. J.; Kurylo, M. J. *J. Phys. Chem.* **1987**, *91*, 5050.

(21) Le Calve, S.; Hitier, D.; Le Bras, G.; Mellouki, A. *J. Phys. Chem.* **1998**, *102*, 4579.

(22) Yamada, T.; Taylor, P. H.; Goumri, A.; Marshall, P. *J. Phys. Chem. A* **2003**, *107* (in press).

(23) Vasvári, G.; Szilágyi, I.; Bencsura, Á.; Dóbé, S.; Bérces, T.; Henon, E.; Canneaux, S.; Bohr, F. *Phys. Chem. Chem. Phys.* **2001**, *3*, 551.

(24) Sander, S. P.; Friedl, R. R.; DeMore, W. B.; Golden, D. M.; Kurylo, M. J.; Hampson, R. F.; Huie, R. E.; Moortgat, G. K.; Ravishankara, A. R.; Kolb, C. E.; Molina, M. J. *Chemical Kinetics and Photochemical Data for use in Stratospheric Modeling. Supplement to Evaluation 12: Update of Key Reactions*; Jet Propulsion Laboratory, 2000.

(25) Gierczak, T.; Talukdar, R. K.; Herndon, S. C.; Vaghjiani, G. L.; Ravishankara, A. R. *J. Phys. Chem. A* **1997**, *101*, 3125.

(26) Jacob, D. J.; Field, B. D.; Jin, E. M.; Bey, I.; Li, Q. B.; Logan, J. A.; Yantosca, R. M.; Singh, H. B. *J. Geophys. Res.* **2002**, *107*, 10.1029/2001JD000694.